DØnote/3566

November 1998

Study of a J/$\psi \to e^-e^+$ trigger in the forward rapidity region for the DØ upgrade

Arnaud Lucotte

State University of New York at Stony Brook

Abstract

This document reviews the possibilities of a J/$\psi \to e^-e^+$ trigger in the forward region for the upgrade DØdetector. We propose algorithms for both the Level 1 (L1) and the Level 2 (L2) triggers. The present algorithms are based on the combination of the End Calorimeter (EC) and the Forward Pre-Shower (FPS) information. Because of the limited coverage of the tracking system, the use of track information has not been considered so far.

The performance of these algorithms have been determined in terms of J/ψ selection efficiency and QCD trigger rates, using Monte Carlo samples. The events used have been fully reconstructed through the upgrade version of GEANT, including a full simulation of the Forward detector, the inner trackers (CFT and SVT), as well as the calorimeter.

We find that a trigger efficiency around 4-10% can be achieved for J/ψ 's in the forward pseudo-rapidity region $1.5 \leq \eta$. For these numbers, trigger rates are expected to be of the order of 1 kHz at Level 1, and below 50 Hz at level 2 for an instantaneous luminosity of $\mathcal{L} = 2 \times 10^{-32}$.cm^{-2}.s^{-1}. For an integrated luminosity of 2 fb^{-1}, a 5% efficiency corresponds to about 1,500 events coming from $B_d \to J/\Psi K^0_S$ (and $\bar{\mathrm{B}}_\mathrm{d}$) decays .

Contents

1 Introduction

For the DØupgrade, the particle ID will benefit from the presence of pre-showers, located in the central rapidity region (CPS) behind the solenoid magnet, as well as in front of the End Calorimeter cryostat (EC) in the foward region (FPS). Previous studies have been performed on the new possibilities offered by the use of pre-shower detectors at the trigger level (1 and 2) to detect soft electrons issued from J/ψ , with thresholds as low as 2.5-3.0 GeV. Motivations for such studies are twofolds: in one hand to make possible B-physics analyses by selecting large samples of B-meson events; on the other hand to ensure the capability to select large samples of J/ψ particles, that could be used for the calibration of the detectors via the reconstruction of the J/ψ mass.

A first detailed study investigated the possibility of a level 1 (L1) trigger on low p_T electrons from b -quarks in the central region $-1.5 \leq \eta \leq 1.5$ [3]. A combination of both CFT tracks and CPS hits was used and the corresponding trigger rates for $p_T \in [5, 10]$GeV dijets events were computed.

A note by P. Grannis [4] describes the performance of a J/ψ trigger in the central rapidity region, by using a combination of the Central calorimeter and the Central Pre-Shower. In this analysis, efficiencies of the order of 6-10% have been achieved, depending on the calorimeter thresholds. Reasonable trigger rates were obtained both at level 1 (below 1 kHz) and level 2 (less than 50 Hz).

In the forward region however, for $1.5 \leq \eta \leq 2.5$, the CFT low η coverage should not allow to use track information together with the PreShower. In this note we propose algorithms for both level 1 (L1) and level 2 (L2) based on the EC electro-magnetic towers and the FPS information. Trigger efficiencies are estimated as well as the QCD trigger rates for an instantaneous luminosity of $\mathcal{L} = 2 \times 10^{-32}.\mathrm{cm}^{-2}.\mathrm{s}^{-1}$.

2 Monte Carlo samples

2.1 J/ψ cross-section

In $p\bar{p}$ collisions, charmonium particles come predominantly from direct QCD production and from the decay of B mesons. In the present study, we use ISAJET J/ψ events produced via $\chi_c \rightarrow J/\psi$ to simulate the first process; b di-jets events where B_d hadrons are forced to decay into a $J/\psi + K^o_s$ are used to simulate the second. In both cases, J/ψ 's are forced to decay into electron pairs $J/\psi \rightarrow e^-e^+$. The *ISAJET* cards used to generate these events are reported in appendix 1.

Corresponding Monte Carlo cross-sections are reported in Table 1. b dijet events have been generated with jet transverse momentum ranging between $1.0 \leq \mathrm{p_T^{jet}} \leq 80$ GeV/c and pseudo-rapidity between $-4 \leq \eta \leq 4$. J/ψ 's issued from χ_c have been generated by Rick Jesik in the whole acceptance of the detector. The cross-section is also indicated in table 1.

Samples	Dijet $\mathrm{p_T^{jet}}$	η range	$\sigma(\mathrm{b-dijet})$	$\sigma(J/\psi \to e^- e^+)$
$B_d \to J/\psi + K^o$	[1,80] GeV/c	η in $[-4.0, 4.0]$	25.3 μb	0.48 nb
$B_d \to J/\psi + K^o$	[4,80] GeV/c	η in $[-4.0, 4.0]$	13.4 μb	0.34 nb
$\chi_c \to J/\psi + X$	[4,80] GeV/c	η in $[-4.0, 4.0]$	—	17.6 nb (*)

Table 1: *Samples used for the trigger studies. Generated η range with corresponding cross sections are indicated. The detail of the cross-section computation is given in the text. (*) number given by Rick Jesik.*

In the following, we use the Monte Carlo cross-sections to estimate the rates. Starting from the b-dijet production cross-section:

$$\sigma(\mathrm{b-dijet}) \approx 25\mu\mathrm{b}$$

One can derive the expected J/ψ cross-section, knowing:

$$\mathrm{BR(b \to B_d^0) = 39.7\%}\ ,\mathrm{BR(B \to J/\Psi{+}K_s^0)} = (8.9{\pm}1.2){\times}10^{-5} \times\frac{1}{2}\ \text{ and } \mathrm{BR(J/\Psi \to ee) = 6.02\%} \quad \text{[PDG98]}$$

leading us to a total cross-section of:

$$\sigma(\mathrm{B \to J/\Psi + X \to ee + X}) = 0.266\ \mathrm{nb}$$

This total cross-section correspond to a number of events of 14,239, so that each event has a weight of 19 fb/event. Cross-sections quoted in table 1 are computed the same way for the different $\mathrm{p_T}$ samples.

Realistic production cross-sections have been measured at $\sqrt{\mathrm{s}} = 1.8$ TeV and are detailed in [5] [6] and [7] in the central rapidity region, and in [8] in the forward region. These analyses are based on di-muons decays of the $J/\psi \to \mu^+\mu^-$ with muon transverse momentum greater than 4.0 GeV/c.
These studies show a strong dependence of the cross-section in the J/ψ momentum, that is not reproduced by the data. This is particularly true for the prompt J/ψ production, where a tuning of the cross-section $\mathrm{p_T}$ -dependence should be performed to get realistic numbers. As a result, electrons or muons produced by J/ψ decay must, in this case, have their $\mathrm{p_T}$ spectrum corrected. Such correction is not applied in this document.

2.2 Characteristics of the signal

Generated events have been classified depending on the $J/\psi \rightarrow e^- e^+$ source (prompt or B-meson decay) and on their direction in the detector: in the following, "central" refers to J/ψ generated in the rapidity range $|\eta_{J/\psi}| < 1.5$, while "forward" designates J/ψ pointing towards the EC acceptance $1.5 \leq |\eta_{J/\psi}| \leq 4$. For our study, we also need to detect electron pairs in the forward region. This is done by requiring that both electrons issued from the J/ψ have $|\eta| \geq 1.5$. In thxe following, J/ψ characteristics will be shown for these three samples.

2.2.1 Characteristics of generated J/ψ 's

Fig. 2.1 and 2.2 show the rapidity of J/ψ issued from b -hadron decays and direct production respectively.

In B processes, generated J/ψ are produced mostly in the central detector, since only about 1/3 point towards the forward region defined above. Among these, less than 30% have both their electrons contained within this area. These numbers are even smaller for prompt J/ψ production, since around 20% point towards the forward area, with only 6% in total in which the electron pair is also well contained in the forward region.

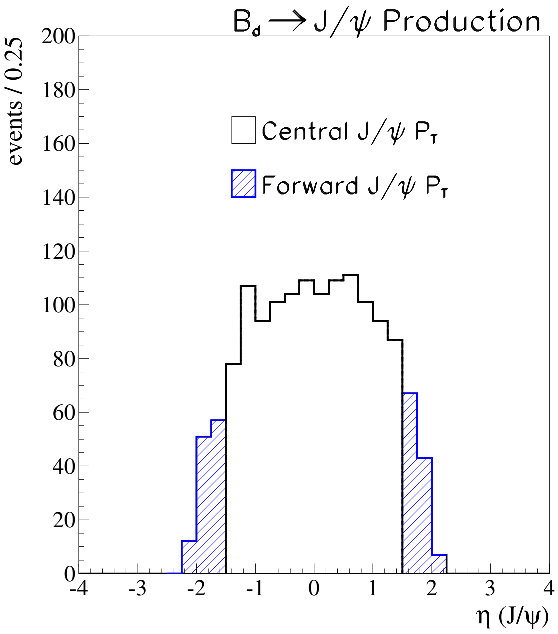

Figure 2.1: *Rapidity of generated* J/ψ *issued from b-quarks events.*

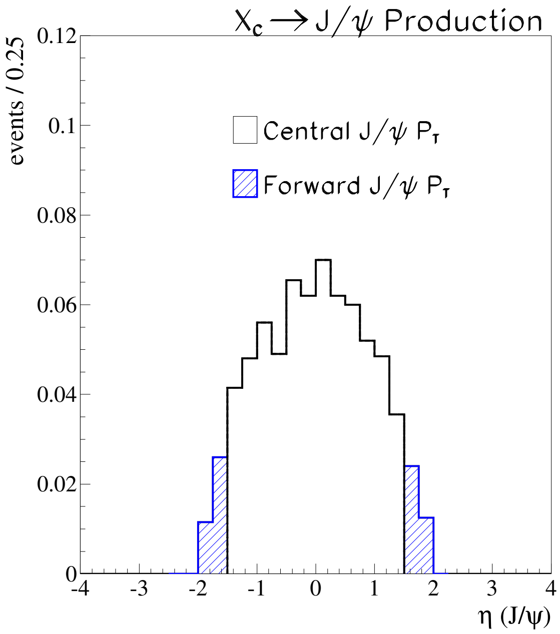

Figure 2.2: *Rapidity of generated* J/ψ *issued from* χ_c *decays*

J/ψ transverse momenta are represented in Fig. 2.3 and 2.4. In B-meson decays, J/ψ 's are produced with a momentum between $2.0 \leq p_T \leq 15$ GeV/c, with a mean value around 4.6 GeV/c. As expected forward candidates have smaller momentum with an average value of 4.1 GeV/c and a somewhat broader distribution.

In prompt J/ψ production, distributions are peaked to lower values of p_T compared to the previous ones. Central J/ψ 's are centered around 4.0 GeV/c for both central and forward samples as well. Distributions in this processus are much tigher than in B-meson decays, where J/ψ 's are produced within jets. One notices that some corrections should be applied to these distributions, making them broader than they appear from the MC [9].

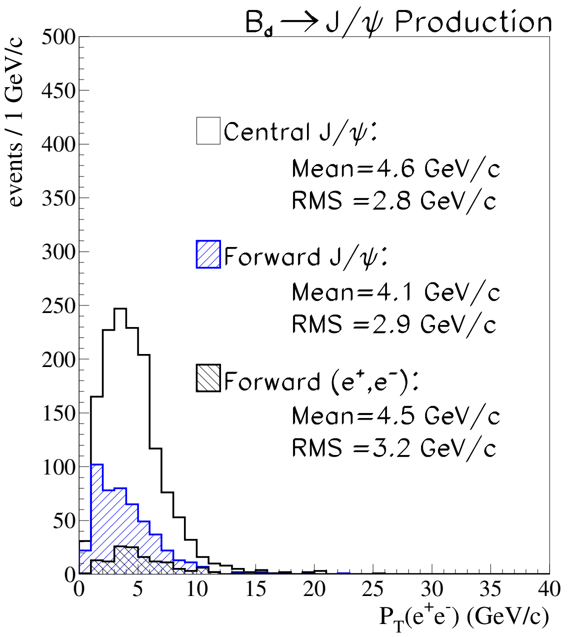

Figure 2.3: *Transverse momentum of generated J/ψ issued from b-quarks events.*

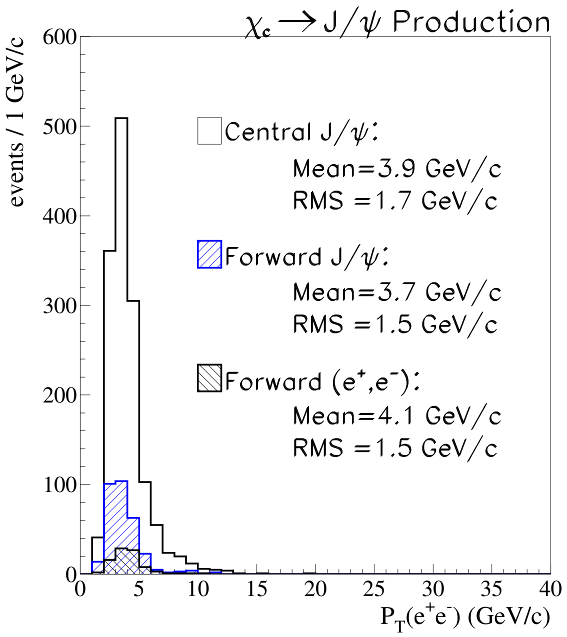

Figure 2.4: *Transverse momentum of generated J/ψ issued from χ_c decays.*

From these plots, it turns out that any J/ψ trigger with J/$\psi \rightarrow e^- e^+$ has to be based on the detection of very low p_T electrons. This remark is specially relevant for the forward region, where p_T spectrum are peaked below 4 GeV/c in both kind of J/ψ 's.

2.2.2 Characteristics of the electrons

As seen previously the energy carried by the J/ψ is relatively small in average. As a result, the transverse momentum of the electrons is expected to be small.

Fig. 2.5 and Fig. 2.6 show the transverse momentum of the electrons resulting from the J/ψ decays. In both production modes, the average electron transverse momentum ranges between 2.0 and 5.0 GeV/c, with a peak around 2.5 GeV/c. No significant difference between forward and central region is seen.

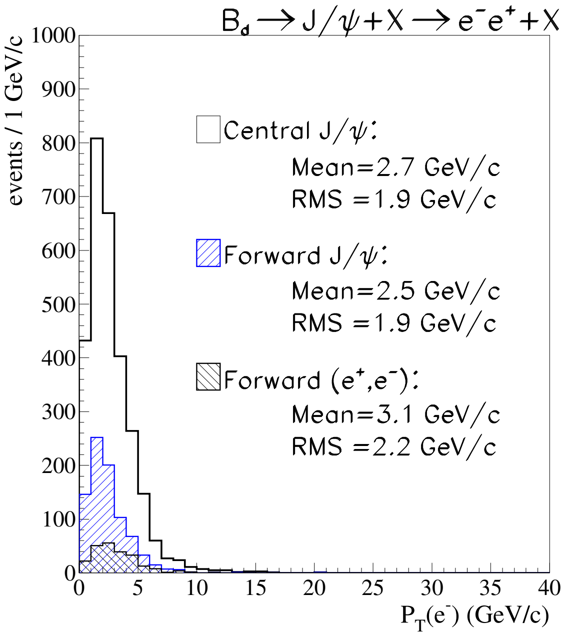

Figure 2.5: *Transverse momentum of the electron produced by the decay of the* J/ψ *in b-quarks events.*

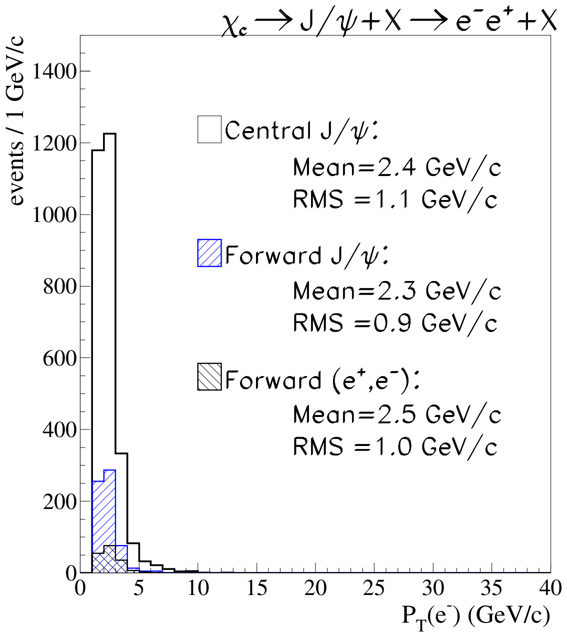

Figure 2.6: *Transverse momentum of the electron produced by the decay of the prompt* J/ψ *'s.*

The opening angles of the electron pair coming from J/ψ are shown in Fig. 2.7 and Fig. 2.8. As expected, the angle may be as wide as 160^o when considering the sample in the whole acceptance. However forward produced electron pairs tend to be more collimated than central ones: in B-meson decays, electrons are distributed within a cone of $\approx 50^o$ while in the prompt production, electron pairs tend to be even more collimated, with forward electrons contained within a 40^o cone. This property may be used in the trigger algorithm, to reduce the search for electron pair within 180 degrees in ϕ in the central region for instance (at L1). This requirement should indeed allow us to reduce background coming from accidental pair fakes present in the dijet samples.

Finally, electron pseudo-rapidity η_e is displayed in Fig. 2.9 and Fig. 2.10. In B-meson events, about 70% of the forward J/ψ have an electron outside the forward acceptance. This number is reduced for prompt J/ψ which are more collimated. This also shows that forward J/ψ have one electron pointing toward the Central region 40% of the time.

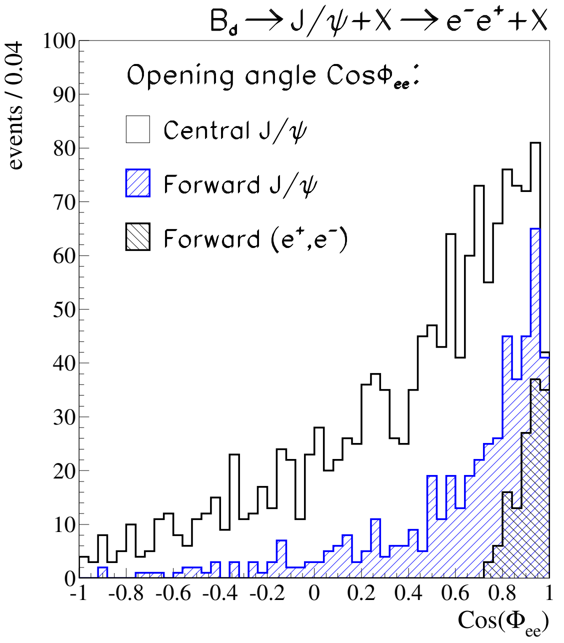

Figure 2.7: *Cosine of the opening angle of electrons coming from b-hadron* J/ψ *decays.*

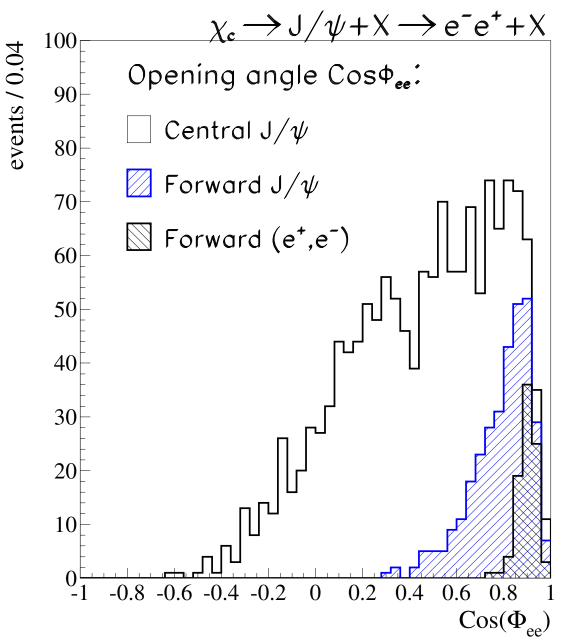

Figure 2.8: *Cosine of the opening angle of electrons coming from $\chi_c \to J/\psi$ decays.*

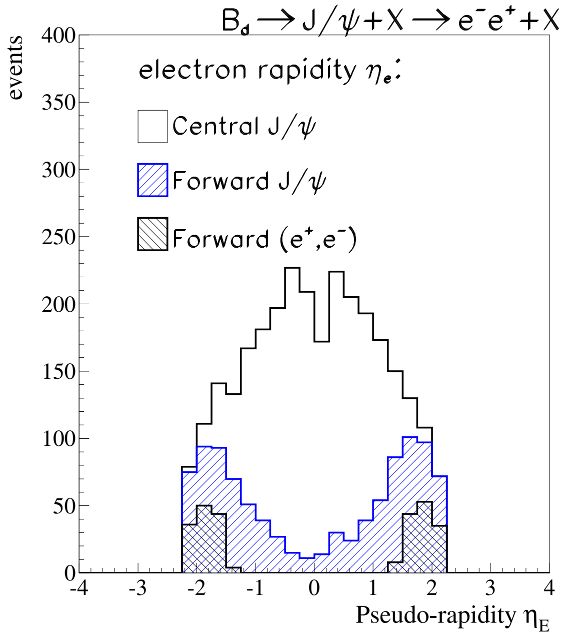

Figure 2.9: *Pseudo-rapidity of electrons (either e^- or e^+) issued from* J/ψ *in b-quark events.*

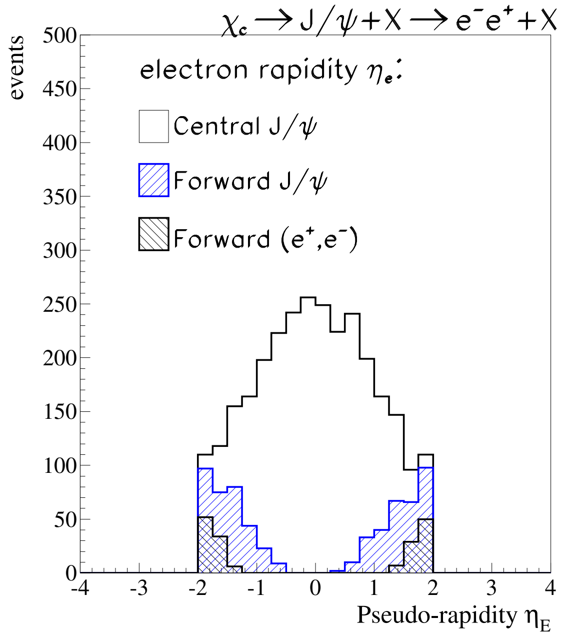

Figure 2.10: *Pseudo-rapidity of electrons (either e^- or e^+) issued from prompt* J/ψ *events.*

2.3 Dijet cross-sections

QCD dijet trigger rates have been evaluated using the cross-sections reported in table 2. We used dijet events produced by ISAJET overlaid with 2 extra minimum bias interactions. This number corresponds to the average number of extra interactions expected for a luminosity of $\mathcal{L} = 2 \times 10^{32}$ with a 99-bunch configuration. MinBias interactions are modelled with low $\mathrm{P_T}$ dijet events generated using ISAJET.

Range in $\mathrm{P_T}$	σ (μb)
02-10 GeV/c	56,590
10-20 GeV/c	543.0
20-40 GeV/c	37.3
40-500 GeV/c	1.8

Table 2: *Dijet Cross sections from samples generated with ISAJET.*

2.4 Geometrical acceptance for a forward trigger

The acceptance of "forward J/ψ 's" is defined as follows. We keep an event if:

- generated J/ψ 's decay into electrons, each with $\mathrm{p_T^e} \geq 1.5$ GeV/c. Below this value, no electron may be detected in the detectors at the trigger level.
- generated J/ψ 's point toward a region corresponding to a polar angle $9.0^o \leq \theta_{\mathrm{gen}}^{\mathrm{J}/\psi} \leq 26^o$ or $154^o \leq \theta_{\mathrm{gen}}^{\mathrm{J}/\psi} \leq 171^o$

The first requirement allows us to compare the results with the numbers quoted for the muon channel in [11]. The second condition ensures that both the FPS and the EC EM are traversed, as illustrated in 3.11. The FPS is composed with 16 modules of 22.5 degrees each, and covers the rapidity region $1.5 < \eta < 2.5$.

The number of such events in our study is: $\mathrm{N_0} = 457$. This sample contains events in which both electrons are pointing towards the forward region (44%), as well as events in which one electron is out of bound (56%). In the following, the numbers quoted for the trigger efficiency are defined as:

$$\epsilon_{\mathrm{trg}} = \frac{\mathrm{N_{sel}}}{\mathrm{N_0}}$$

The current algorithm is devoted only to the case where two electrons are detected in the forward region. This means that our trigger efficiency starts at 44% of the generated sample.

3 Level 1 Trigger

In this section, after describing the constraints encountered at Level 1 (L1), we present an L1 algorithm. Trigger efficiencies for both b-hadronic decay J/ψ 's and prompt J/ψ 's modes are then derived. Corresponding QCD rates are also estimated.

3.1 Constraints at Level 1

For this study, we consider that data are taken with a with 99-bunch configuration and an instantaneous luminosity of:

$$\mathcal{L} = 2 \times 10^{-32}.\mathrm{cm}^{-2}.\mathrm{s}^{-1}$$

The acceptance rate for the global L1 is set between 6 and 10 kHz, limited by tracking and calorimeter readout as well as dead time minimization. Any L1 decision must be taken within 4.2 μs, which sets the limits of the complexity of the algorithms used at this level. The technical design of the trigger system as well as the data load are studied in [12], [2] and [10]

Given the high energy physics program scheduled for the run II, the total estimated rates at L1 [12] leads us to consider 1.5 kHz as the total Band Width available for J/ψ triggering. A J/$\psi \to \mu\mu$ trigger takes about 400 Hz at L1 [11]. This leaves us with around 1kHz for both central and forward J/$\psi \to \mathrm{e}^-\mathrm{e}^+$ trigger

3.2 Trigger algorithm

The L1 trigger algorithm is based on the combination of both the EC and the FPS detectors. Basically, it is required that two towers be hit in the EC with an EM transverse energy above a certain threshold CALEM. It is also asked that at least one electron candidate is found in the FPS detector, in the same quadrant where the EC candidate is found. No finer matching may be defined at L1, mainly because of timing constraint that allows us to use only an ECEM tower signals summed over a quadrant (8 towers in ϕ and 4 in η[14]). Other options of L1 FPS/ECEM combinations have been tested with no significant improvement [12].

As for the definition of an electron in the FPS, the algorithm is detailed in [12]. It is based on the detection of an energy cluster in the shower layer, coincident with a MIP signal in front of the lead converter, as shown in Fig. 3.11.

Finally, to reduce further the QCD background, we use the fact that the electron pair coming from the J/ψ decay is quite collimated. We therefore require that two FPS candidates be separated by no more than ± 3 modules.

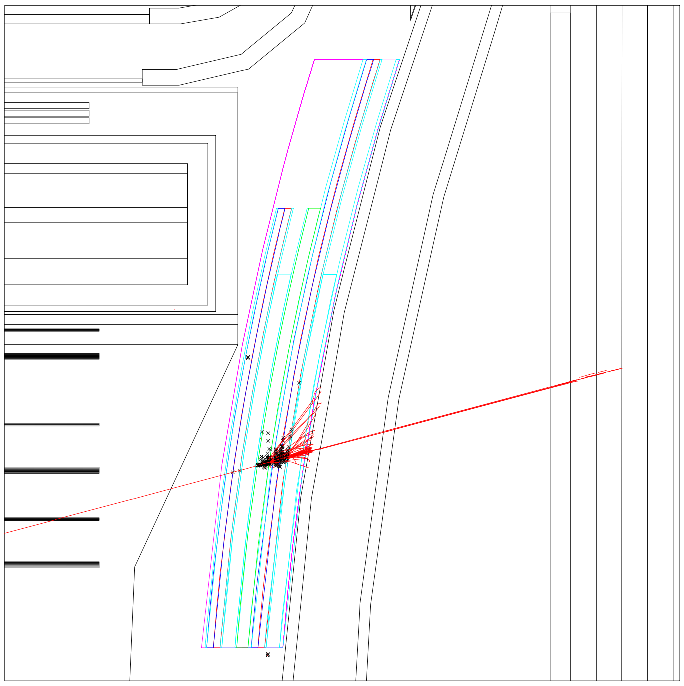

Figure 3.11: *Electron traversing the FPS detector. The triggering is based in a cluster measured in the shower layers in coincidence with a MIP deposition in front of the lead converter. The threshold defining the strip in a cluster is FPSEM, and is varied from 5 to 10 MIPs.*

To summarize, the L1 algorithm requires:

1. Two EC EM towers above a threshold CALEM.

2. At least one electron candidate in the FPS, located in front of a hit tower within the same EC quadrant. An FPS candidate is defined as a cluster of strips, each with

an energy above FPSEM behind the lead converter [2], in coincidence with a MIP deposition in front of the lead.

3. The difference $|\Delta\Phi(e,e)|$ between two FPS candidates is within ± 3 modules, corresponding to $\pm 67.5^o$.

These points are detailled in the following sections.

3.3 ECEM Calorimeter thresholds

The value chosen for CALEM drives the QCD trigger rates. Figure 3.12 displays the trigger rates as a function of the CALEM threshold in the [2.0,4.0]GeV range. QCD Rates being very sensitive to small variations of CALEM, we apply the smallest possible variation of the threshold available at L1. This value corresponds to the Least Significant Bit (LSB) used for the EM section of the trigger tower, which is 1/4 GeV.

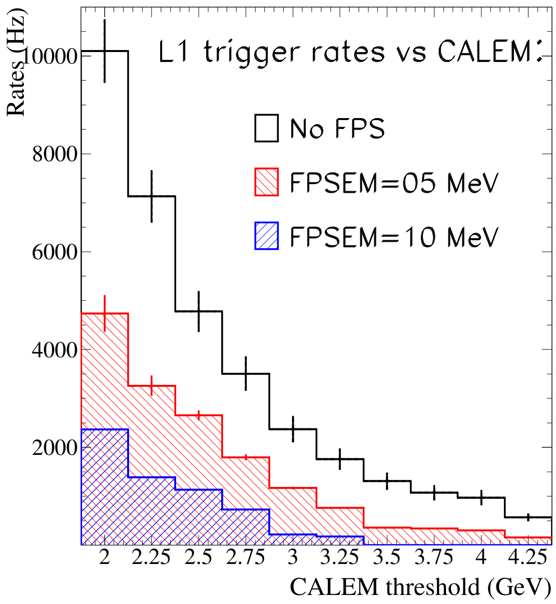

Figure 3.12: *Di-electron trigger Rates as function of CALEM. The first case is based on using the EC alone; the 2nd and 3rd require a confirmation by two FPS candidates with a threshold of 5 and 10 MIPs. Erros bars indicate statistical uncertainty only.*

From Fig. 3.12 it appears obvious that no di-electron trigger based on the EC alone may be defined for CALEM ≤ 2.5 GeV: below this value, prohibitive QCD rates are indeed expected. However, the addition of the FPS information allows us to improve the rejection of the QCD background by a factor 2 to 5. Thus, for CALEM=2.5 GeV and FPSEM=10 MIPs, the rejection factor is raised by a factor 5 when one requires the coincidence of the EC depositions with FPS signals located in the same quadrant. For this value of CALEM, trigger rates are expected to be below 3 kHz with FPSEM=5 MIPs and below 1 kHz with FPSEM=10 MIPs.

As a conclusion, it seems possible to set calorimeter as well as FPS thresholds so that reasonable trigger rates are observed at L1. The calorimeter thresholds must be set above 2.5 GeV while in the FPS thresholds ranging between 5 or 10 MIPs may be used. One notices that the use of the FPS information however appears crucial to significantly reject QCD background at L1.

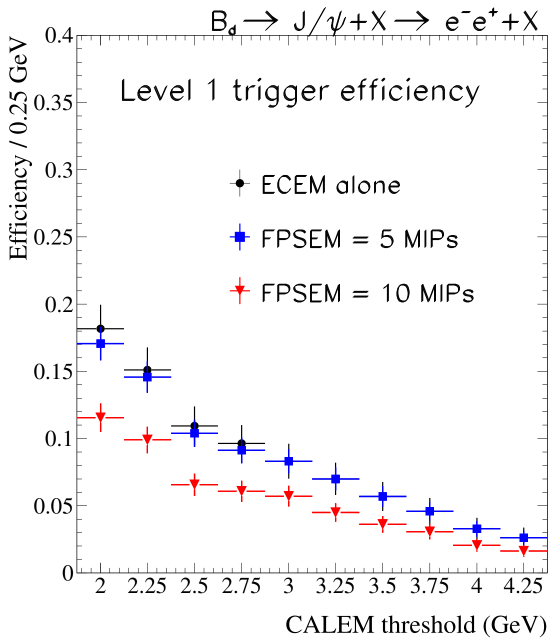

Figure 3.13: *Di-electron trigger efficiency as function of CALEM. The first case is based on using the EC alone; The second one uses the coincidence with FPS candidates within the same quadrant, with a cluster threshold of 5 and 15 MIPs.*

The J/ψ selection efficiency $\epsilon_{\rm trg}$ sensitivity to the CALEM threshold has also been investigated. Fig. 3.13 displays this efficiency $\epsilon_{\rm trg}$ as function of the CALEM threholds. It also compares the situation where one requires only two EM towers above CALEM, to the one where the FPS confirmation is required. In this figure, FPS candidates are defined without FPS information (circle), with FPSEM=5 MIPs (square) and FPSEM=15 (triangle) MIPs thresholds. Selection efficiencies $\epsilon_{\rm trg}$ vary from 18 to 4% as the calorimetric threshold is raised from 2.0 to 4.0 GeV. This is the direct consequence of the electron p_T distribution shown in Fig. 2.5, which peaks below 3.0 GeV/c. However, the use of realistic values of CALEM $\geq$ 2.75 GeV leads to acceptable efficiencies about $\epsilon_{\rm trg} = 10\%$.

The relative efficiency of the FPS with respect to the EC appears close to 100% for the highest values of CALEM and for FPSEM below 5 MIPs. Degradation in signal trigger efficiency are observed for high values of FPSEM like 15 MIPs, while the usual range is between [5,10] MIPs.

3.4 FPS/ECEM matching

Only a crude match of the ECEM and the FPS candidates is allowed at L1. The algorithm requires that at least one FPS candidate is matched to an EC quadrant, where a signal is detected. Fig. 3.14 and Fig. 3.15 show the effect of such requirements on the signal efficiency as well as the trigger rates as a fuction of CALEM.

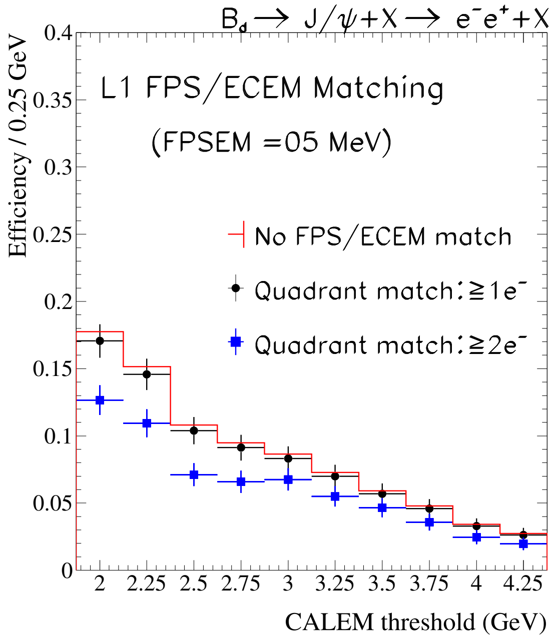

Figure 3.14: *Effect on the signal efficiency of a single/double match between the ECEM and the FPS detectors*

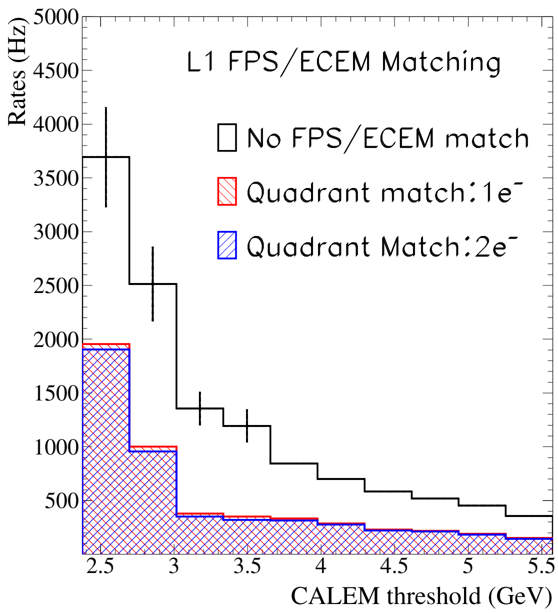

Figure 3.15: *Effect on the trigger rates of a single/double match between the ECEM and the FPS detectors*

Where no match between the detectors is required, efficiencies are at the order of 16 to 5 % as shown previously. Requiring the match of at least one FPS candidate within the same quadrant of an EC signal makes almost no difference in terms of efficiency (less than 2%). However, asking for a double match between the FPS and the ECEM within quadrant degrades the efficiency by 2 to 5% depending on CALEM, whereas at the same time, no further rejection is observed in the QCD rates. These results are explained by the L1 trigger efficiency for a single low p_T electron, which is around 80% [12] and decreases with the electron p_T (selected by lower values of CALEM). As the dijet rejection is not affected by the requirement of single/double matching, we therefore require in the following that at least one FPS candidate (in total) match the EC signals.

3.5 FPS threshold

The definition of an electron candidate in the FPS depends mainly on the threshold set to detect the energy cluster behind the lead converter. As shown in [12], the single electron trigger efficiency also depends on the particle's energy.

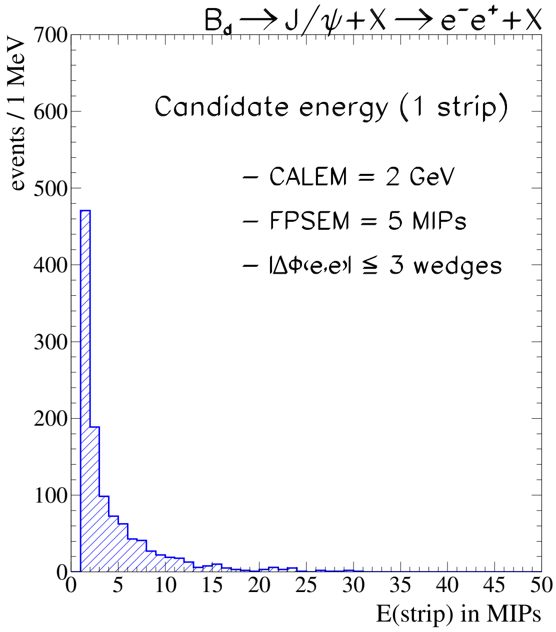

Figure 3.16: *Energy of strip candidates as measured in the shower layer of the FPS. A coincidental MIP deposition is already required in the layers in front of the converter. The following values have been chosen: CALEM=2 GeV, $\Delta\Phi(\mathrm{e},\mathrm{e}) \leq 3$ wedges.*

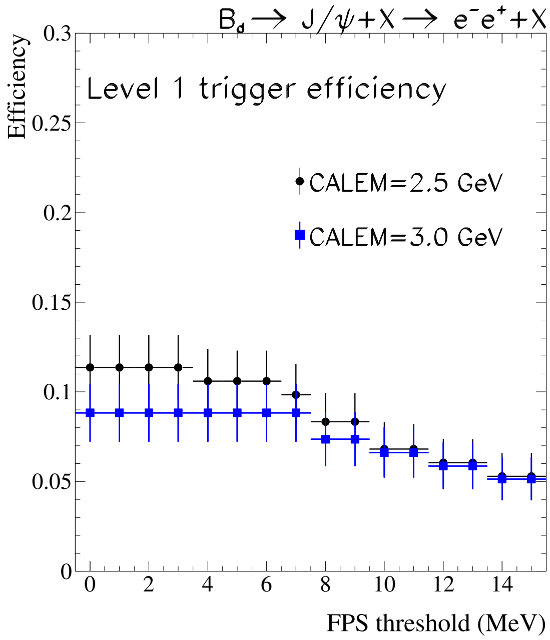

Figure 3.17: *Trigger efficiency for two electrons coming from* J/ψ *with* $\mathrm{P_T} \geq 2$ GeV/c. *Results are shown for two values of CALEM set to 2.0 and 2.5 GeV and for the separation cut* $\Delta\Phi(\mathrm{e},\mathrm{e}) \leq 3$ *(see next section).*

Fig. 3.16 represents the energy as measured in one strip by an electron candidate in the FPS. For this candidate, a MIP deposition before the converter is already required, as defined in [12]. Fig.3.17 displays the L1 trigger efficiency computed for two values of CALEM (2 and 2.5 GeV) as function of the cluster threshold, FPSEM, ranging between 0 and 15 MIPs. The reasonable range of variation for FPSEM is [5-10] MIPs. Between these values, single electrons of all energy may be detected in the FPS detector: according to [12] a 10 MIPs threshold indeed removes around 30% of low $\mathrm{p_T} \approx 2$ GeV/c electrons. On the other hand, a 3 MIPs threshold does not reject efficiently light or neutral hadrons backgrounds (like π^0 conversions) present in the jets and which convert before the FPS is reached.

Table 3 reports the trigger efficiency as function of FPSEM.

FPSEM (MIPs)	0.0	2.0	5.0	8.0	10.0	15.0
Efficiency $\epsilon_{\rm trg}$ (%)						
CALEM=2.50 GeV	11.4±1.8	11.4±1.8	10.6±1.7	8.3±1.6	6.8±1.3	5.3±1.3
CALEM=2.75 GeV	10.9±1.7	10.9±1.7	9.4±1.5	7.2±1.4	6.5±1.3	5.0±1.2
CALEM=3.00 GeV	8.8±1.6	8.8±1.6	8.8±1.6	7.3±1.4	6.6±1.3	5.1±1.2

Table 3: *J/ψ trigger efficiency $\epsilon_{\rm trg}$ as a function of the FPSEM threshold. Results are reported for CALEM=2.5 GeV, CALEM=2.75 GeV and CALEM=3.0 GeV.*

For CALEM=2.75 GeV, an efficiency of $\epsilon_{\rm trg}$ ≈11% is found with low FPS threshold $FPSEM \leq 4$ MIPs. Results are stable for FPSEM below 5 MIPs but become somewhat sensitive to FPSEM between 8-15 MIPs. Raising FPSEM from 5 to 10 MIPs results in a loss of a 30% of the selected events, for a final efficiency around $\epsilon_{\rm trg} = 6.5\%$ at 10 MIPs.
For CALEM=3.0 GeV, less than 9 % of the J/ψ 's are selected by the EC towers alone. The application of the FPSEM=10 MIPs removes about 25% of these events, with a remaining $\epsilon_{\rm trg} = 6.6\%$.

3.6 Electron pair separation

We display in Fig. 3.18 the $\Delta\Phi(\mathrm{e,e})$ separation, in number of wedge(s) (or sector(s)), between the two candidates found in the FPS. For this plot, when there is more than 2 electron candidates (jet residues), all the combinations have been considered.

The electron pairs are expected to be collimated, as shown in the preliminary studies in Fig. 2.7. In Fig. 3.18, candidate pairs indeed turn out to be contained within 3 modules, corresponding to 67.5^o. The (flat) tail of the distribution may come from the FPS candidates issued from the jet content. Fig. 3.19 shows the trigger efficiency $\epsilon_{\rm trg}$ sensitivity to the cut on the $\Delta\Phi$ separation of the electrons. $\epsilon_{\rm trg}$ drops when one requires both candidates to be within only 1 or 2 modules. However, it is rather unsensitive to the cut for higher values. We set this cut at 3 modules between the two candidates:

$$\Delta\Phi(\mathrm{e}^-\mathrm{e}^+) = 3 \text{ wedges}$$

in order to optimize QCD background rejection. For this value, less than a percent of signal is lost.

It should be noticed however that this requirement does not bring much of improvement (a few ≈ 50 Hz), which is within statistical uncertainties.

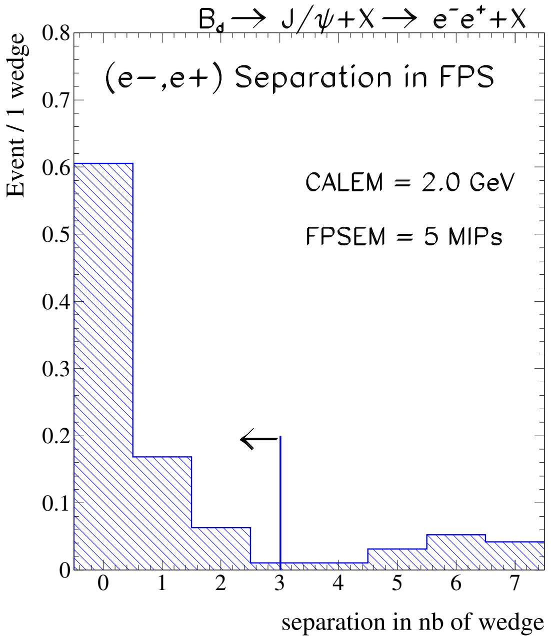

Figure 3.18: *Difference $\Delta\Phi$(e,e) between the two FPS candidates in signal events. The unit is in number of wedge, with 1 wedge = 22.5^o.*

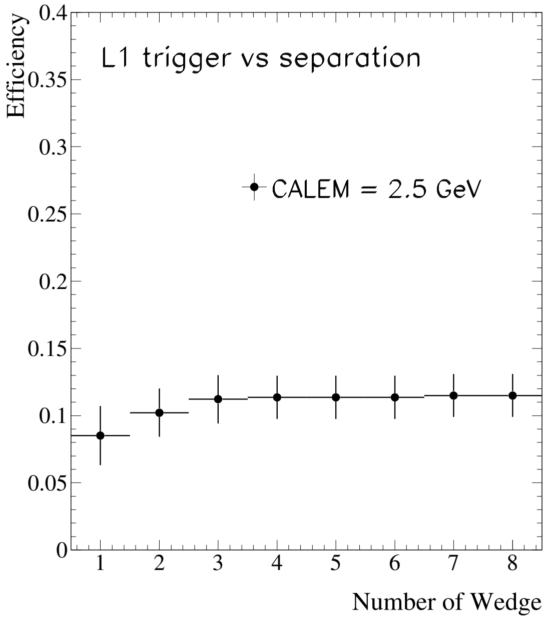

Figure 3.19: *Sensisitity on the signal of the variation of the $\Delta\Phi(e,e)$ cut between the two FPS candidates.*

3.7 Results at L1

The results shown so far apply for events in which both electrons have a generated $p_T^e \geq$ 1.5GeV/c (corresponding roughly to $p_T^{J/\Psi} \geq 3.0$ GeV/c on average). The signal efficiency depends strongly on this requirement, since the electron selection is directly affected by the E_T threshold in the calorimeter. Figure 3.20 shows the trigger efficiencies for several intevals of p_T , for CALEM= 2.5 GeV.

As expected, the trigger efficiency ϵ_{trg} obtained is quite good for very energetic J/ψ 's (tail of the p_T distribution in Fig. 2.3), with around $\epsilon_{trg} = 30\%$ of selected J/ψ 's for $p_T \geq$ 6.0 GeV/c. For lower p_T J/ψ 's, electrons are not detected with a CALEM threshold set at 2.5 GeV, which results in an efficiency below 8%.

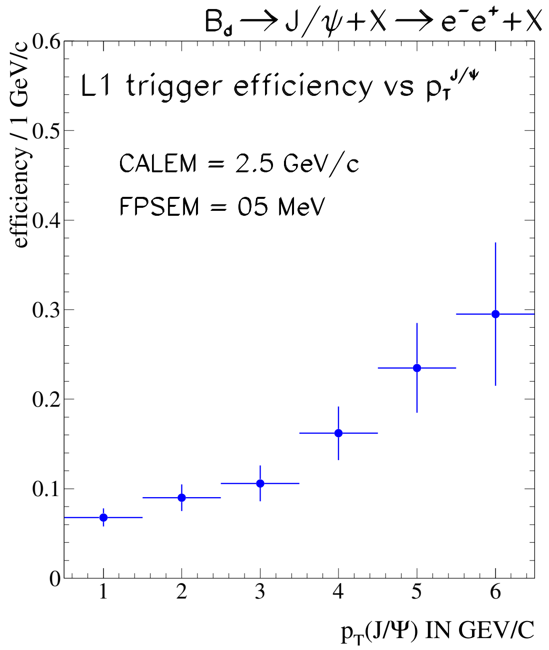

Figure 3.20: *Trigger efficiency for generated J/ψ momentum above 1,2,...and 6 GeV/c. The results are shown for CALEM = 2.5 GeV and FPSEM = 5 MIPs. Error bars correspond to statistical uncertainty only.*

As a conclusion, a (simple) trigger algorithm based on the combination of the EC and the FPS information available at L1 has been developped for J/ψ pointing towards the forward region $1.5 \leq \eta \leq 2.5$. This algorithm does not use any tracking information.
The signal efficiency ϵ_{trg} turns out to be driven by the value of CALEM, the threshold applied on the EM section of the EC towers. and by the value of FPSEM, the threshold set to detect electron showers in the FPS detector.

The algorithm, applied on dijet samples, leads to trigger rates around and below 1.0 kHz for CALEM greater than 2.75 GeV and FPSEM above 5-10 MIPs. The corresponding trigger efficiencies for $P_T \geq 2.75$ GeV/c J/ψ 's range between 5 and 11 %.

4 Level 2 Trigger

4.1 Constraints at Level 2

The Level 2 (L2) trigger is based upon a L1 decision. A L2 decision has to be taken within a few hundred micro-seconds, which leaves us an appreciable amount of time to use more complexe algorithm. The other constraint comes from the L2 Band Width. The total Accept rate at L2 is around 1kHz. This means that $\approx$ 100 Hz has to be considered as a maximum for $J/\psi \to e^- e^+$ triggers.

The design and performance of a L2 trigger for the FPS is described in [10],[12],[13]. It is based on two levels: an intermediate level composed with a set of FPS-specific pre-processors, that translate the FPS signals into η, ϕ; a global level, that is devoted to the fine matching of individual EC towers with FPS candidates.

4.2 Trigger algorithm

The L2 algorithm is based upon the L1 decision. Provided that the event passes the L1 trigger, the total energy of the electron candidate, its isolation energy and its location are computed and used to reconstruct the invariant mass of the electron pair candidates. Basically:

1. **Isolation criterium:** $\mathrm{F_{ISO}} \leq \mathrm{ISO}$, where the definition of $\mathrm{F_{ISO}} = \mathrm{E_T^{ISO}}/\mathrm{E_T^{TOT}}$ is defined as the ratio of the energy measured in the neighbors around the seed tower (= tower above CALEM)

2. **Angular separation** between electron candidates: $\mathrm{Cos}(\Phi_{ee}) > 0.8$ as given by the EC towers (passing CALEM) candidates

3. **Invariant Mass of electron pair:** $\mathrm{MASS_{INF}} \leq \mathrm{M}(e^-, e^+) \leq \mathrm{MASS_{SUP}}$ where angles and the electron energy $\mathrm{E_T^{TOT}}$ are provided by the EC alone

The energy $\mathrm{E_T^{ISO}}$ and $\mathrm{E_T^{TOT}}$ are defined in the following. In the current algorithm, angles and energy of the electron candidates are used, thus allowing us to reconstruct the invariant mass of the present pair(s). Both angles and energy information are provided by the EC alone, the FPS detector being used as a confirmation signal of the energy deposition in front of the hit towers. Indeed, the fact that in some cases we do not have a confirmation signal for both electrons prevent us from using the angular information as given by this detector. However, as the uncertainty in the invariant mass reconstruction is expected to be dominated by the energy reconstruction in the EM towers, we do not forsee any significant improvement by using the angular information from the FPS. The invariant mass is reconstructed according to:

$$M(e^-,e^+) = \sqrt{2 \times (|p_{e^+}.p_{e^-}| - \vec{p_{e^+}}.\vec{p_{e^-}})}$$

where one defines: $p_{e^-} = E_T^{TOTe-}/\sin(\theta_{e^-})$ and $\vec{p_{e^-}}$ are computed from θ_{e-}, ϕ_{e-} and E_T^{TOTe-} given by the location of the seed 0.2×0.2 EC towers (tower above CALEM).

One notices that the precision on the invariant mass reconstruction strongly depends upon the definition of E_T^{TOT} and E_T^{ISO}. The next two sub-sections are devoted to the definition of these variables, chosen to optimize the mass reconstruction precision and the QCD background rejection.

4.3 ECEM Electron energy: E_T^{TOT}

Contrary to L1, the L2 allows us to use of the analog information coming from the individual EC EM towers. This information is here used to optimize the discrimination based on shape comparisons between low p_T electron and background coming from the jet(s). We compare here several definitions for the total energy of the electron candidate. For each EM tower above the L1 threshold CALEM, we compute:

1. st definition: $E_T^{TOT} = E_T^{seed}$ where E_T^{seed} is the energy of the central EM tower
2. nd definition: $E_T^{TOT} = E_T^{seed} + \sum_{j=1}^{4} E_T^{j}$ where the summed energy of the four 1st neighbors is added to the seed energy, namely towers with $E_T^{\Phi_{i+1},\eta_i}$, $E_T^{\Phi_{i-1},\eta_i}$, $E_T^{\Phi_i,\eta_{i-1}}$ and $E_T^{\Phi_i,\eta_{i+1}}$
3. rd definition: $E_T^{TOT} = E_T^{seed} + \sum_{j=1} E_T^{CALEM/2}$ where the energy of the towers above half the threshold is added to the seed energy

The probability density functions are shown in Fig. 4.21, 4.22 and 4.23 for the 3 definitions. On these plots, the comparison with the invariant mass reconstructed in dijet events is also shown.

We choose the definition that optimizes the reconstruction of the invariant mass of the J/ψ while preserving a high discriminating power against the QCD background. Table 4 reports the values obtained for the reconstructed mass $< M(e^-,e^+) >$, together with the discriminating power of each of these definitions. $< M(e^-,e^+) >$ is given by a fit of the distribution in the mass window [2.0-6.0]GeV/c^2. The sigma of the fit is also reported. The discriminating power is defined as the ratio

$$R = \epsilon_S/\sqrt{\epsilon_B}$$

where ϵ_S is the efficiency with wich the signal is selected within the mass window $[2.5 - 6.0]$ GeV/c^2, and ϵ_B the background efficiency estimated on the same mass range.

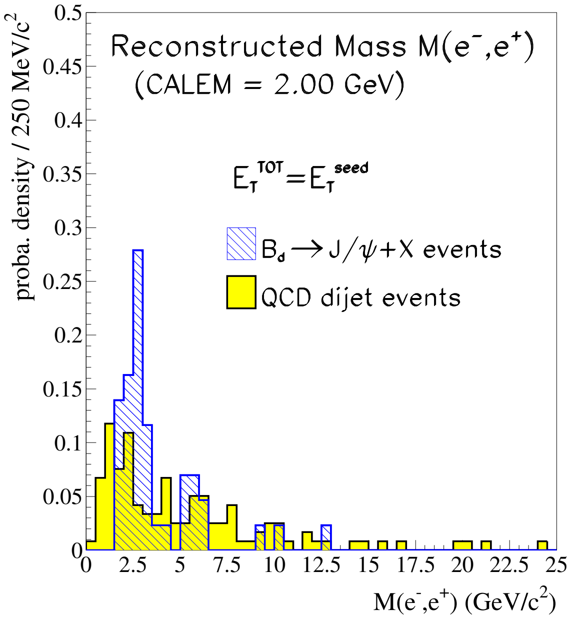

Figure 4.21: *Reconstructed J/ψ for the definition 1 of E_T^{TOT} of the electron energy. Also shown is the comparison with the invariant mass reconstructed for dijet events*

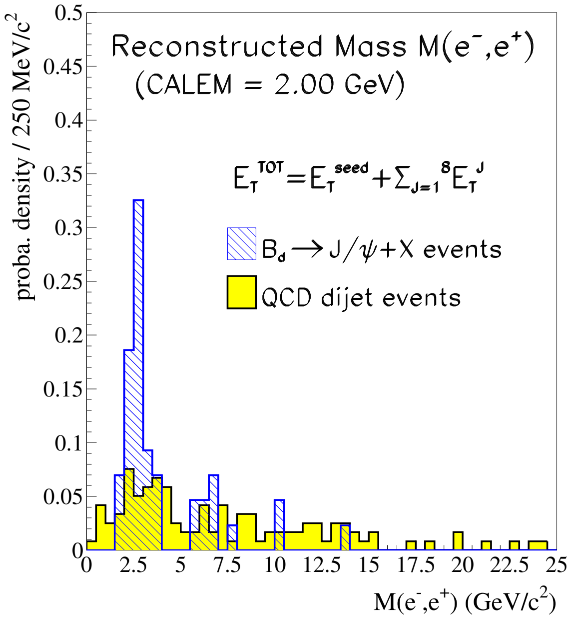

Figure 4.22: *Reconstructed J/ψ for the definition 2 of E_T^{TOT} of the electron energy. Also shown is the comparison with the invariant mass reconstructed for dijet events*

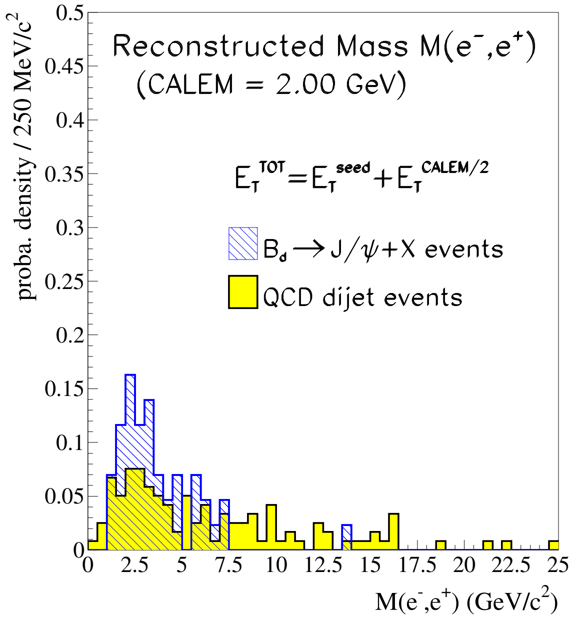

Figure 4.23: *Reconstructed J/ψ for the definition 3 of E_T^{TOT} of the electron energy. Also shown is the comparison with the invariant mass reconstructed for dijet events.*

E_T^{TOT} Definition	$< M(e^-, e^+) >$ in GeV/c^2	R in $[2.5 - 5.0]$ GeV/c^2		
		ϵ_S	ϵ_B	R
Def(1)	2.51±0.63	0.74	0.38	1.20
Def(2)	2.62±0.53	0.75	0.37	1.22
Def(3)	2.48±2.15	0.72	0.37	1.18

Table 4: *Invariant Mass reconstructed from* J/ψ *samples and discriminating power within the mass window [2.5-5.0] GeV/*c^2 *against dijets. For these numbers, CALEM = 1.5 GeV.*

The following conclusions are drawn:

- the 1^{st} definition tends to underestimate the energy left by the electron, which results in an systematic underestimation of $M(e^-, e^+)$. As the reconstructed mass from dijet events is concentrated around lower values. This is reflected in the shift in the mean value towards the lower masses. Signal efficiency is around 74% and the discriminating power is around the same as for the 2^{nd} definition

- for the 3^{rd} definition, the reconstructed mass distribution is much broader (σ 4 times the other definitions), resulting in a small loss of discriminating power of $M(e^-, e^+)$ against the QCD continous background

- the 2^{nd} definition of E_T^{TOT} also allows the signal to be selected more efficiently (about 75%) than the two other definitions. The σ given by the fit is the smallest one and the discriminating power the largest.

These results are stable when the mass window is made vary. We therefore choose the 2^{nd} definition for the total energy of the electron:

$$E_T^{TOT} = E_T^{seed} + E_T^{\Phi_{i+1},\eta_i} + E_T^{\Phi_{i-1},\eta_i} + E_T^{\Phi_i,\eta_{i-1}} + E_T^{\Phi_i,\eta_{i+1}}$$

4.4 ECEM Electron isolation

We define the isolation energy $\mathrm{E_T^{ISO}}$ of the electron candidate so that the reconstructed J/ψ mass is optimized. We compare two definitions of $\mathrm{E_T^{ISO}}$:

1. st definition: $\mathrm{E_T^{ISO}} = \mathrm{E_T^{TOT}} - \mathrm{E_T^{seed}}$
2. nd definition: $\mathrm{E_T^{ISO}} = \mathrm{E_T^{TOT}} - \mathrm{E_T^{seed}} - \mathrm{E_T^{CALEM/2}}$ where $\mathrm{E_T^{CALEM/2}}$ stand for the sum of all the towers above half the threshold around the seed tower.

We find that a better discrimination is found in the first definition. Figure 4.24 displays the ratio $F_{ISO} = \frac{E_T^{ISO}}{E_T^{TOT}}$ in this case. A cut at $\mathrm{F_{ISO}} = 0.4 - 0.5$ for each EC candidate allows a good rejection of the background while keeping an acceptable signal efficiency.

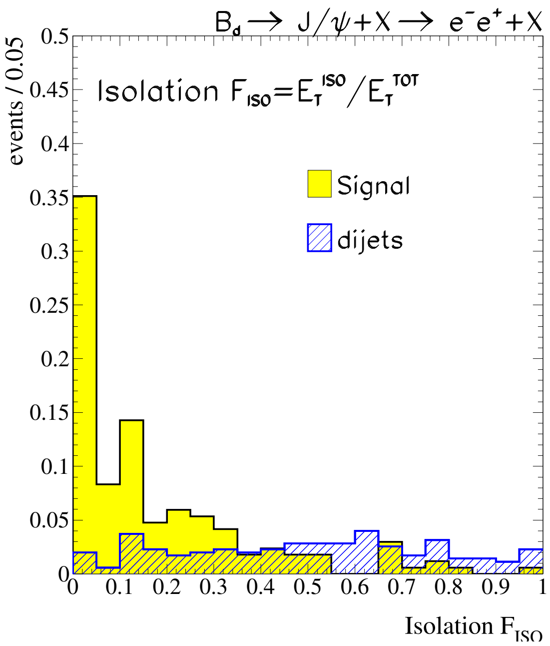

Figure 4.24: *Distribution of the* $\mathrm{F_{ISO}}$ *isolation parameter for signal and dijet backgrounds.*

In the following, all the results are derived using the 1^{st} definition.

Figures 4.25 displays the sensitivity of the signal efficiency to the isolation threshold $\mathrm{F_{ISO}}$ varying from 0.0 to 1.0. The efficiency is particularly affected for values $\mathrm{F_{ISO}} \leq 0.5$. This is explained by the facts that we deal here with very low $\mathrm{p_T}$ electrons, and that this requirement is applied on both EC candidates.

Figure 4.26 shows the effects of such cut in the QCD trigger rates obtained for CALEM=2.5 GeV. This figure presents the sensitivity to the isolation criterium alone, since the results do no include the FPS matching nor the invariant mass cut. The application of a requirement $F_{ISO} = 0.5$ allows us to reduce the dijet rates by a factor 1/3.

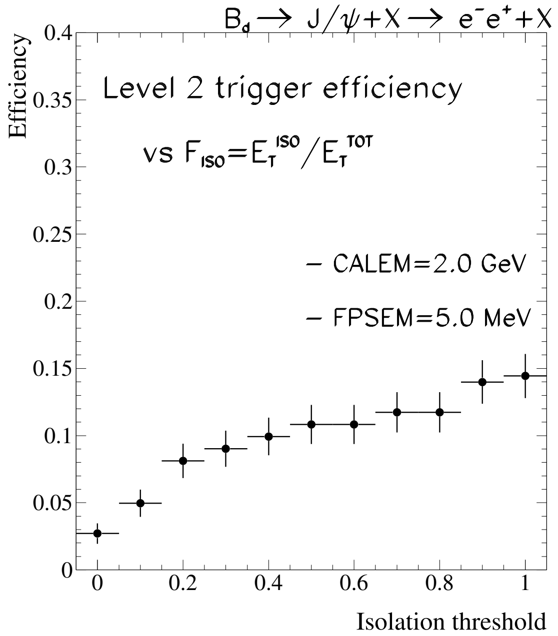

Figure 4.25: *Selection efficiency for the signal as function of the isolation threshold as defined in the text. CALEM is set to 2 GeV, FPSEM at 5 MIPs and the Mass window ranges between 2 to 6*$\mathrm{GeV/c^2}$.

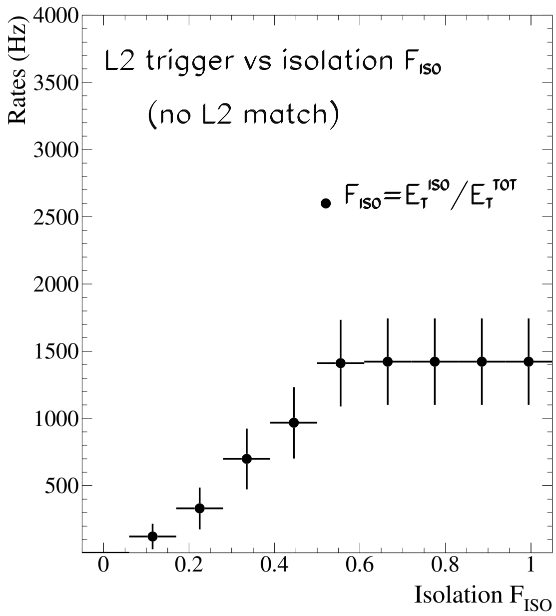

Figure 4.26: *L2 trigger rates as function of the L1 EC threshold CALEM. The results are shown for two values of F_{ISO}. No other L2 requiremens is applied (no FPS matching and no mass cut)*

One notices that for low values of CALEM, the efficiency of the isolation cut is reduced, compared to what is observed for CALEM > 2.5 GeV. This is explained by the fact that lower CALEM values lead to select jet particles with lower p_T, which do not deposit much energy around the seed tower. As this CALEM increases, the isolation requirement becomes more and more efficient, and leads to rejection factor of the order of 1.5-2.0.

4.5 FPS/ECEM matching

At Level 2, a fine matching between the EC individual trigger towers and the FPS detector is made possible. The information from the EC is sorted out according to the 0.2×0.2 segmentation in the (η, ϕ) space. For the FPS, a lookup table is accessed at the L2 Preprocessor, that is used to translate the (u,v,wedge) information into η, ϕ [13].

As we require only one electron matched at L1, we also ask for a single match between the FPS candidates and the EC towers. Figure 4.27 shows the effect of such requirement on the signal efficiency, while Fig. 4.28 represents the sensitivity of the L2 rates to the matching, as a function of the L2 CALEM threshold.

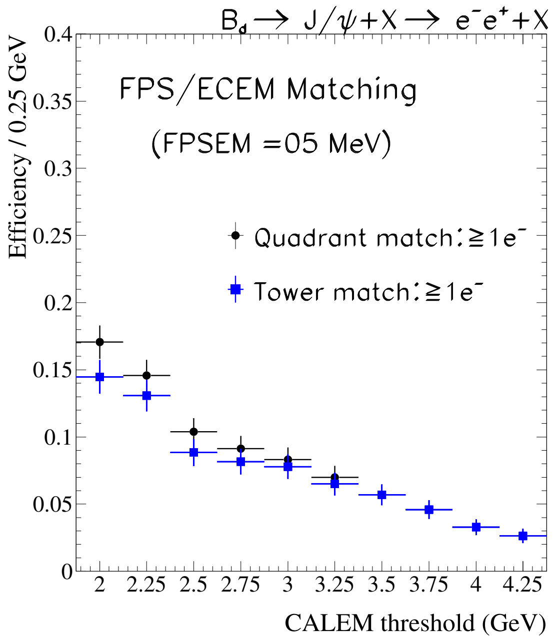

Figure 4.27: *Comparison of the effects of the L1 match and the L2 match on the signal efficiency as function of the L1 CALEM threshold.*

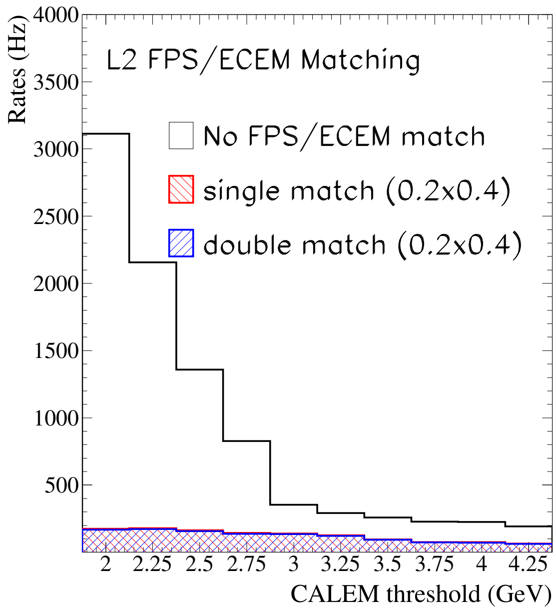

Figure 4.28: *L2 rates with/without L2 matching as function of CALEM. The isolation requirement is applied. No mass cut is applied.*

From the signal efficiency standpoint, no significant degradation is observed as we require a L2 matching between the FPS and the EC trigger towers. For lower values of CALEM <2.5, signal looses only a few percent. However, for reasonable values of CALEM, no effect is seen.

From the rates standpoint, the matching brings a significant rejection, since a single electron match gives results in a reduction by a factor 4 of the rates at CALEM=2.75 GeV. This rejection factor is better for lower CALEM values, because charged hadrons (for instance)

in jets are not associated to any FPS clusters. From Fig. 4.28 it also appears that no improvement is observed as two matched electrons are required. At most, an extra rejection of 20 Hz is seen, but is compatible with our uncertainty.
In the following, a single L2 electron match is required.

4.6 Electron pair Invariant Mass

The invariant mass of the electron candidates, confirmed by the FPS, is used as an efficient cut to remove QCD background. As the invariant mass reconstructed from dijet events shows a strong dependence in the threshold CALEM, we report results for different values of this threshold.

4.6.1 Sensitivity to MASSCUT

The selection efficiency depends upon the mass window defined to select J/ψ candidates. Fig. 4.29 and Fig. 4.30 show the dependence in the lower and upper bound of the mass window.

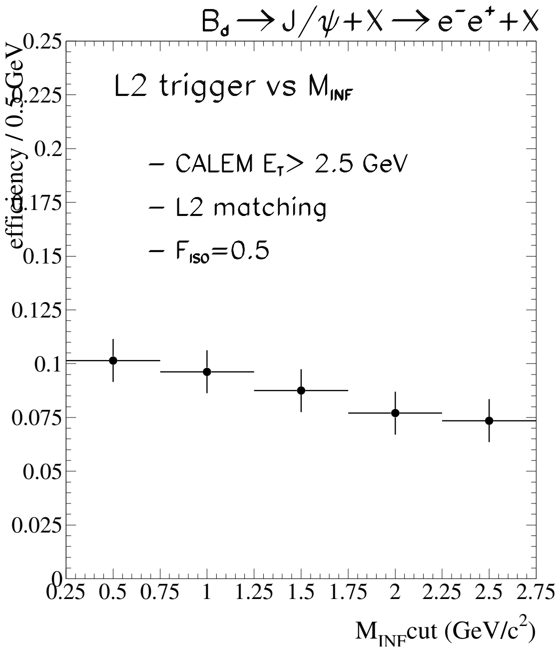

Figure 4.29: *Sensitivity to the lower bound of the mass window used to select candidates*

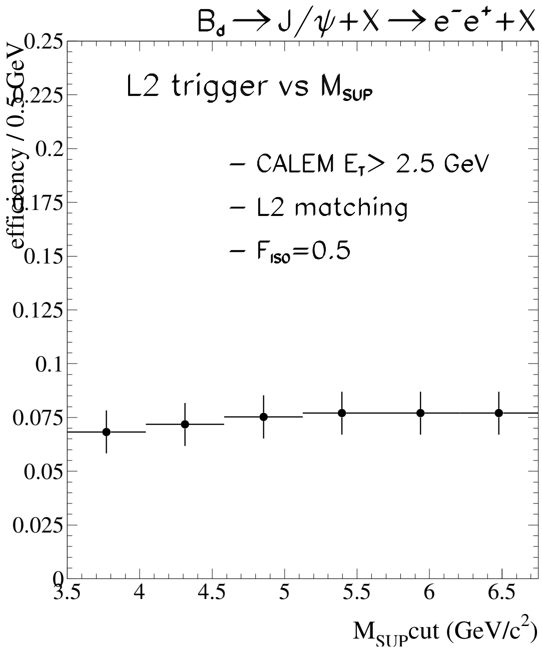

Figure 4.30: *Sensitivity to the upper bound of the mass window used to select candidates*

The use of the lower bound is crucial since it rejects all the lower masses reconstructed in jet events (fake electrons, combinatory). At the same time, it does not affect too much

the signal efficiency, although variations of 25% are seen as MASS_INF is raised from 1.5 to 2.5 GeV/c^2. A reasonable value for MASS_INF = 2.0 GeV/c^2 is chosen.
As for the upper bound, again we choose a value that minimizes the degradation of the efficiency while keeping a high background rejection. The dependence in the value of MASS_SUP is quite important, since a non negligible part of the mass spectrum is above 4 GeV/c^2. We choose to set this cut at 6.0 GeV, thus limiting the loss in signal efficiency while improving the QCD background rejection.

4.6.2 Sensitivity to ECEM threshold

The CALEM threshold used at L1 drives the rejection rates of the QCD background. We analyse here the dependence of the reconstructed invariant mass $M(e^-, e^+)$ in CALEM threshold, ranging in between 2.00 to 2.50 GeV. Fig.4.31 and 4.32 display the probability density of $M(e^-, e^+)$ for two reasonable values of the EC threshold: CALEM=2.25 GeV and CALEM=2.50 GeV. These thresholds allow to keep L1 di-electron rates at an acceptable level.

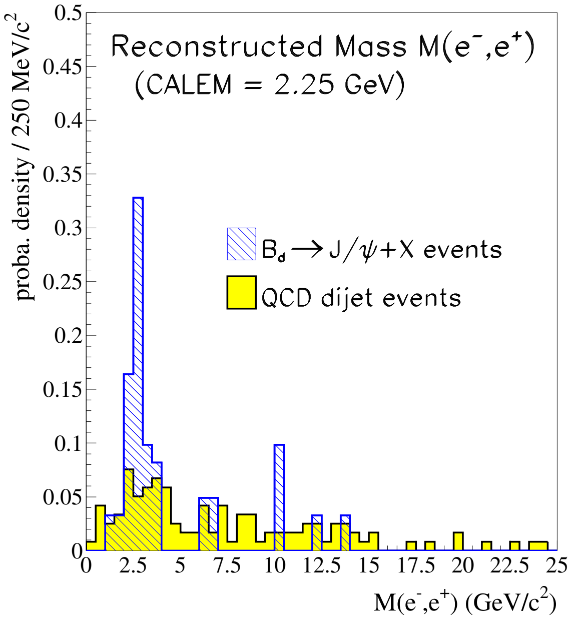

Figure 4.31: *Probability density for reconstructed $M(e^-, e^+)$ for signal and dijet events. CALEM is set at 2.25 GeV.*

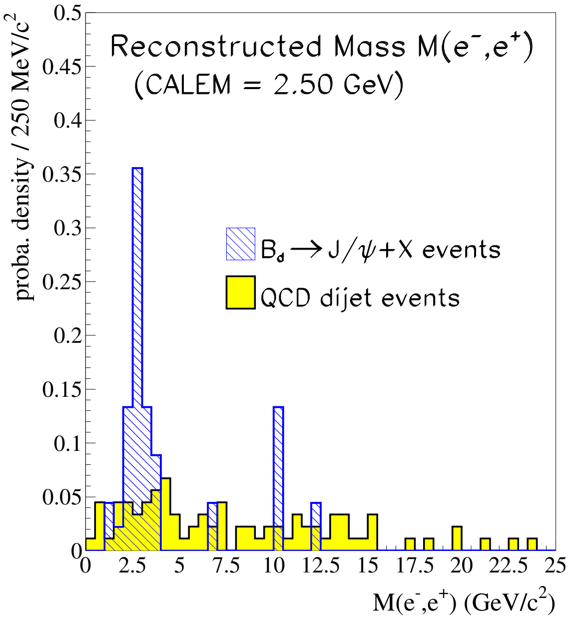

Figure 4.32: *Probability density for reconstructed $M(e^-, e^+)$ for signal and dijet events. CALEM is set at 2.50 GeV.*

Both the signal and dijet background are compared, to take the dependence of dijet events in the CALEM threshold. The values of the reconstructed mass for the signal have been fitted with a gaussian between 2 and 6 GeV/c^2. They are reported in Table 5.

CALEM (GeV)	2.00	2.25	2.50
$M(e^-, e^+)$ (MeV/c^2)	2,619	2,687	2,800
σ(MeV/c^2)	430	450	480
$\chi^2/d.o.f$	0.03	0.03	0.03

Table 5: *Results of the fit of the reconstructed Invariant Mass for different values of the L1 CALEM threshold. The mass window is set to [2.0-6.0] GeV/c^2*

The reconstructed mass turns out to be in reasonable agreeement with the generated $M_{J/\psi}$ but suffers from limited statistics of our samples. However the following conclusions can be drawn:

- the results are stable for the different values of CALEM, with a well apparent peak in the 2-6 GeV/c^2 window
- the width of the reconstructed mass distributions is affected by the limited statistics associated with increasing CALEM threhold. However, reasonable values of the width are obtained, ranging between 400 and 800 MeV/c^2.

4.7 Results at L2

Figure 4.33 shows the L2 rates as function of CALEM between 2.0 and 4.0 GeV. L2 Trigger rates are found to be below 50 Hz for reasonable values of CALEM, ie: CALEM$\geq$2.5 GeV. These results are explained by:

- the requirement of at least one matched electron between the individual EC trigger towers and the FPS clusters. For CALEM>2.5GeV, this accounts for a factor 2 to 4 in the rates rejection.
- the isolation requirement brings a rejection of 1.5-2.0 depending on CALEM
- the cut on the reconstructed invariant mass accounts for a factor 2-3.

The final numbers match the L2 Band Width constraints, which requires a maximum below 100 Hz for $J/\psi \to e^- e^+$ triggering.

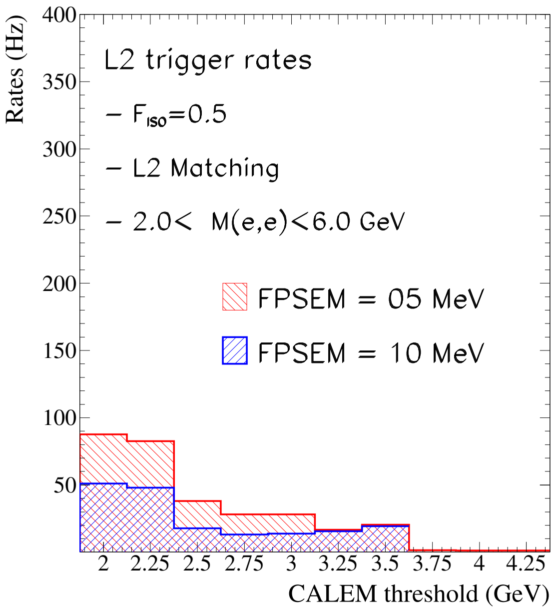

Figure 4.33: *L2 trigger rates as function of CALEM. The isolation cut, the single electron matching and the mass cut are appliedas indicated on the plot.*

At the same time, for similar values of CALEM, signal efficiencies range 6-10% for B meson J/ψ 's. The main cause of signal rejection is the CALEM threshold, that prevents us from selecting very low p_T electron to maintain acceptable L1 rates. Our algorithm is moderately sensitive to the FPSEM threshold, that defines the electron cluster in the FPS detector. However, trigger efficiency depends strongly on the matching requirements: A double match (two FPS clusters and two EC towers) reduces the efficiency by 40%. This leads us to use a single match.

5 Conclusion

We studied an algorithm devoted to the triggering of $J/\psi \to e^- e^+$ events. We determined L1 and L2 trigger efficiencies as well as the corresponding QCD trigger rates. We used Monte Carlo samples, where the events are fully reconstructed through the upgrade version of GEANT, including a full simulation of the Forward detector, the inner trackers (CFT and SVT), as well as the calorimeter.

We find that a trigger efficiency around 4-10% can be achieved for J/ψ 's in the forward pseudo-rapidity region $1.5 \leq \eta$. With an efficiency of 5% and a integrated luminosity of 2 fb^{-1}, we thus expect $\approx 1,500$ J/ψ coming from $B_d \to J/\Psi K_s^o$ (and $\bar{B}_d$) decays.
For these numbers, trigger rates are expected to be of the order of 1 kHz at Level 1, and below 50 Hz at level 2 for an instantaneous luminosity of $\mathcal{L} = 2 \times 10^{-32}.cm^{-2}.s^{-1}$.

The main limitation of such triggering is the dijet rates expected at L1. With runs devoted to B physics or calibration, we therefore conclude that J/ψ triggering is possible in the electron channel in the Forward region of the detector.

A ISAJET card file for $B_d \to J/\psi + K_S^0$ production

Generates Bd → Jpsi+K0s
2000.,10000,0,0/
TWOJET
BEAMS
'P','AP'/
JETTYPE1
'BT','BB'/
JETTYPE2
'BB','BT'/
PT
1.5,80.,1.5,80./
Y
-4.0,4.0,-4.0,4.0 /
FORCE
250,441,230 /
FORCE
441,12,-12 /
NOPI0
T
NOETA
T
TMASS
173. /
SEED
19610405100307/
NTRIES
4000/
END
STOP

B ISAJET card file for $\chi_c \to J/\psi + X$ production

```
GENERATE CHIS
1800.000, 5000, 0, 0/
CHIS
BEAMS
P','AP'/
PT
1.5 50.0 -1.0E09 -1.0E09/
-3.0 3.0 -3.0 3.0/
LAMBDA
0.4/
POMERON
4,4/
FORCE1
443 441 10 0 0 0
FORCE1
444 441 10 0 0 0
FORCE1
445 441 10 0 0 0
FORCE1
441 -12 12 0 0 0
EVOLVE
HADRON
TRIES
500000
SEED
95793467891.
END
STOP
```

References

[1] "TDR of the Central Preshower detector for the DØupgrade"

[2] "TDR of the Forward Preshower detector for the DØupgrade" J. Kotcher et al.

[3] Level1 trigger on low pt electrons from b-quark decays in the central region, Y. gershtein, DØnote 3249.

[4] "J/ψ trigger in the central region", P. Grannis, DØnote 3506

[5] J/ψ and ψ(2S) Production in ppar collisions at $\sqrt{s} = 1.8$ TeV The CDF coll., Fermilab-Pub-97/024-E

[6] Production of J/ψ mesons from χ_c meson decays in ppb collisions at $\sqrt{s} = 1.8$ TeV, Fermilab-Pub-97/026-E

[7] DØcollaboration, S. Abachi at al., Phys. Lett. B370,239(1996)

[8] DØcollaboration, Editorial Board 041, http://www-d0.fnal.gov/www_buffer/eb/eb_041/eb_041_01.html

[9] A. Zieminski, private communications

[10] TDR in preparation, Fred Borcherding et al.

[11] DØnote 3354, Frederic Stichelbaut et al.

[12] DØnote 3493. "Definition of a L1 electron and photon trigger with the FPS", A. Lucotte and M. Bhattacharjee

[13] "Perfomance of an electron trigger at Level 2", DØnote in preparation, M. Bhattacharjee

[14] Paul Grannis, Dan Edmunds, private communication